LRIG1 inhibits STAT3-dependent inflammation to maintain corneal homeostasis

Takahiro Nakamura,[1,2] Junji Hamuro,[1] Mikiro Takaishi,[3] Szandor Simmons,[4] Kazuichi Maruyama,[1] Andrea Zaffalon,[5] Adam J. Bentley,[6] Satoshi Kawasaki,[1] Maho Nagata-Takaoka,[1] Nigel J. Fullwood,[6] Satoshi Itami,[7] Shigetoshi Sano,[3] Masaru Ishii,[4] Yann Barrandon,[5] and Shigeru Kinoshita[1]

[1]Department of Ophthalmology, Kyoto Prefectural University of Medicine, Graduate School of Medicine, Kyoto, Japan. [2]Research Center for Inflammation and Regenerative Medicine, Doshisha University, Kyoto, Japan. [3]Department of Dermatology, Kochi Medical School, Kochi University, Nankoku, Japan. [4]Laboratory of Cellular Dynamics, World Premier International Research Center Initiative–Immunology Frontier Research Center, Osaka University, Osaka, Japan. [5]Laboratory of Stem Cell Dynamics, School of Life Sciences, École Polytechnique Fédérale de Lausanne (EPFL), and Centre Hospitalier Universitaire Vaudois (CHUV), Lausanne, Switzerland. [6]Biomedical and Life Sciences, School of Health and Medicine, Lancaster University, Lancaster, United Kingdom. [7]Department of Regenerative Dermatology, Graduate School of Medicine, Osaka University, Osaka, Japan.

Corneal integrity and transparency are indispensable for good vision. Cornea homeostasis is entirely dependent upon corneal stem cells, which are required for complex wound-healing processes that restore corneal integrity following epithelial damage. Here, we found that leucine-rich repeats and immunoglobulin-like domains 1 (*LRIG1*) is highly expressed in the human holoclone-type corneal epithelial stem cell population and sporadically expressed in the basal cells of ocular-surface epithelium. In murine models, LRIG1 regulated corneal epithelial cell fate during wound repair. Deletion of *Lrig1* resulted in impaired stem cell recruitment following injury and promoted a cell-fate switch from transparent epithelium to keratinized skin-like epidermis, which led to corneal blindness. In addition, we determined that LRIG1 is a negative regulator of the STAT3-dependent inflammatory pathway. Inhibition of STAT3 in corneas of *Lrig1*$^{-/-}$ mice rescued pathological phenotypes and prevented corneal opacity. Additionally, transgenic mice that expressed a constitutively active form of STAT3 in the corneal epithelium had abnormal features, including corneal plaques and neovascularization similar to that found in *Lrig1*$^{-/-}$ mice. Bone marrow chimera experiments indicated that LRIG1 also coordinates the function of bone marrow–derived inflammatory cells. Together, our data indicate that LRIG1 orchestrates corneal-tissue transparency and cell fate during repair, and identify LRIG1 as a key regulator of tissue homeostasis.

Introduction

In mammals, most external information is accumulated through visual systems, and integrity of the cornea is well known to be indispensable for good vision (1). During evolution, nature has found a way to develop a well-ordered visual system to maintain corneal tissue transparency and homeostasis. The cornea is a unique avascular and transparent epithelial tissue that harbors stem cells that control homeostasis and tissue regeneration after injury (2, 3). However, the homeostatic turnover of corneal epithelial tissue can become disrupted depending on the severity of damage to the corneal epithelium, resulting in collateral chronic inflammation and impaired tissue repair (4, 5). These inflammation-associated processes reportedly interfere with corneal transparency and the cornea's barrier function (6).

It is well known that stem cells work to maintain the self renewal and repair of tissues and organs (7, 8). Under normal conditions, the corneal epithelial tissue accommodates the homeostatic turnover of corneal stem cells, which is essential for postinjury tissue regeneration. Previous studies have reported that corneal epithelial stem cells reside in the basal layer of the limbal zone of the peripheral cornea (9, 10). The corneal epithelial stem cell system is one of the most clearly defined systems and is therefore an ideal model for investigating the role of regulatory molecules associated with stem cell tissue repair (2, 3). However, the molecular interplay between corneal epithelial stem cells and other players with critical roles in the regulation of tissue repair has yet to be elucidated.

Barrandon et al. previously reported the existence of 3 types of epidermal keratinocytes with different self-renewal capacities (11). Similar behavior has subsequently been reported for corneal keratinocytes (12). Holoclones (stem cells) have the highest reproductive capacity, while in paraclones (transient amplifying cells), terminal differentiation is observed within a few generations. However, the molecular mechanism and gene expression profile of holoclone-type stem cells are entirely unknown.

Leucine-rich repeats and immunoglobulin-like domains 1 (LRIG1) is a transmembrane glycoprotein recently reported as a potential master regulator of epidermal and intestinal epithelial stem cells (13–17). However, there are no reports to date that address the tissue-specific function of LRIG1 in the cornea. The findings of this present study demonstrate that LRIG1 was highly expressed in the holoclone-type corneal epithelial stem cells and that it was essential for the cell-fate maintenance of corneal epithelium during tissue repair. Loss of *Lrig1* impaired wound-induced corneal stem/progenitor cell replacement and resulted in a cell-fate change from corneal to keratinized epithelium. Intriguingly, we found that LRIG1 controlled the corneal cell fate during repair by negatively regulating the Stat3-dependent inflammatory pathway. Moreover, corneal cell fate during repair was not only maintained by corneal epithelial stem/progenitor cells, but

Conflict of interest: The authors have declared that no conflict of interest exists.
Citation for this article: *J Clin Invest.* 2014;124(1):385–397. doi:10.1172/JCI71488.

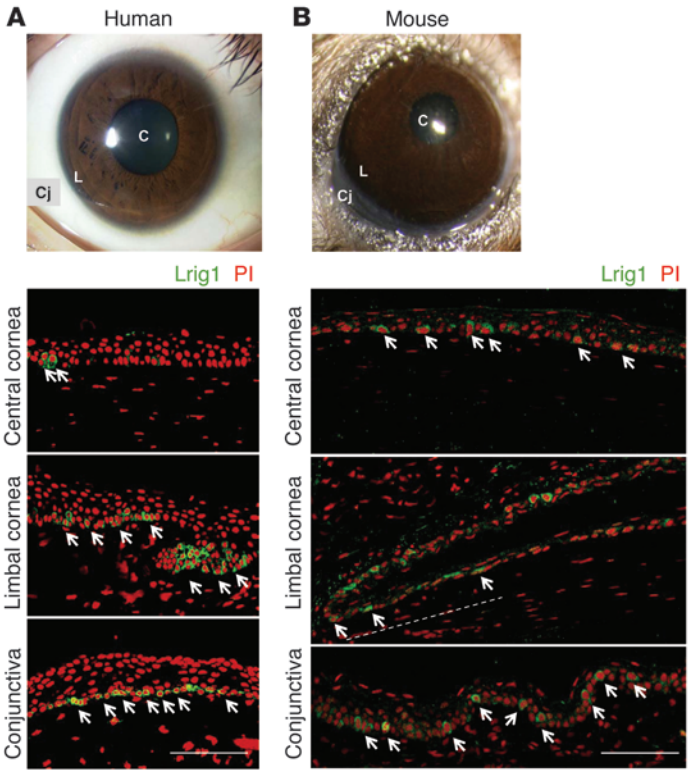

Figure 1
Expression of LRIG1 in the ocular surface epithelium (corneal, limbal, and conjunctival). (**A** and **B**) Slit-lamp photographs of a human eye and a mouse eye. Immunohistochemistry for LRIG1 (green, arrows) in human (10 years) and mouse (3 months) ocular surface epithelium. Nuclei are counterstained with PI (red). The dashed line indicates the limbal area. C, central cornea; L, limbal cornea, Cj, conjunctiva. Scale bars: 100 μm.

also by BM-derived inflammatory cells, whose functions are well-regulated by the LRIG1/STAT3 inflammatory pathway. Thus, the findings of this present study provide new insights into the underlying homeostatic regulation of corneal keratinocyte stem/progenitor cells by LRIG1.

Results

Gene expression profile of holoclone-type corneal keratinocyte stem cells. In order to gain insight into the mechanisms responsible for the homeostasis within epithelial stem cells, we performed gene expression profiling of holoclone-type and paraclone-type human corneal keratinocytes. This led to the identification of 15 genes that were upregulated at least 5-fold in holoclone-type corneal epithelial stem cells (Supplemental Tables 1 and 2; supplemental material available online with this article; doi:10.1172/JCI71488DS1). We next examined the expression pattern of these genes using immunohistochemistry and identified *Lrig1* for further investigation, because LRIG1 was specifically expressed in human limbal basal cells and rarely expressed in the differentiated central corneal epithelium (Figure 1A). In contrast, in mouse eyes, LRIG1 was only found to be sporadically expressed in the basal cells of the ocular surface epithelium (cornea, limbus, and conjunctiva), and immunostaining patterns suggested a cluster (patch) organization (Figure 1B), indicating a strong relationship with epithelial stem/progenitor cell–related molecules (18).

Loss of Lrig1 results in a cell-fate change from corneal to keratinized epithelium. To clarify the biological roles of *Lrig1* in the cornea, we generated *Lrig1*-deficient mice according to our previous protocol (13) and then analyzed their phenotype in detail. During the developmental stage (E15–P10), there were no abnormal phenotypes in the cornea (data not shown). At 3 months of age, neither *Lrig1* WT nor KO mouse corneas elicited abnormal phenotypes, as observed both macroscopically and histologically (Figure 2A). However, corneal epithelial stratification, the number of conjunctival goblet cells, and BrdU-labeled cell ratios (in vitro) tended to be slightly higher in the KO specimens, thus suggesting that *Lrig1* plays a role even in steady-state homeostasis (Supplemental Figure 1). After a latency period of 6 months, *Lrig1*-KO corneas gradually formed corneal plaques with massive neovascularization and intense infiltration of inflammatory cells. Finally, approximately 70% of the *Lrig1*-KO mice developed abnormal corneal phenotypes within 24 months (Figure 2B). Histological examination revealed extensive thickening and pathological keratinization of the corneal epithelium, with inflammation of the underlying corneal stroma (Figure 2A).

To determine the biological characteristics of the corneal epithelial cells, we performed immunohistochemistry for cornea-specific keratin 12 and epidermis-specific loricrin (Figure 3A). While the epithelia of the WT corneas (3, 8, and 12 months) specifically expressed keratin 12, that of the *Lrig1*-KO corneas (3, 8, and 12 months) had gradually lost keratin 12 (Supplemental Figure 2) and gained loricrin expression. These changes were also associated with increased proliferation, as determined by BrdU labeling. This suggests that loss of *Lrig1* results in a cell-fate change from corneal to keratinized epithelium, which leads to the thickening of the epithelium.

Inflammation is a known clinical feature of keratinization-associated blindness, and tissue-intrinsic inflammatory responses recruit hematopoietic cells, as they drive epithelial hyperproliferation via a reciprocal signaling loop (19, 20). Characterization of the inflammatory infiltrates in remodeling tissues of *Lrig1*-KO corneal stroma (12 months) showed pronounced recruitment of CD31-, F4/80-, GR1-, and CD3-positive cells (Figure 3B), while these were completely absent in the normal WT corneal stroma (12 months). This implies that the loss of *Lrig1* results in the intensive infiltration of BM-derived inflammatory cells.

Loss of Lrig1 impairs wound-induced corneal stem cell turnover. Corneal homeostasis is maintained by stem cells, which are responsible for physiological cell turnover and the wound-healing response (2, 3). We hypothesize that the cell-fate switch observed in the *Lrig1*-deficient corneal epithelium is a consequence of an abnormal tissue repair process following injury. To investigate this theory, we performed mechanical corneal-epithelial debridement (2 mm) under a microscope. After wounding the cornea once per week for 3 weeks, all of the KO corneas (3 months) developed intensive inflammation and subsequent corneal opacity, in contrast with the WT corneas (3 months) with normal phenotypes (Figure 4A). This strongly implies that the cell-fate switch of the *Lrig1*-KO cornea is initiated by wound stimulation. We next examined the corneal wound repair process, kinetically, until 7 days after wounding. Slit-lamp examination using fluorescein staining clearly revealed

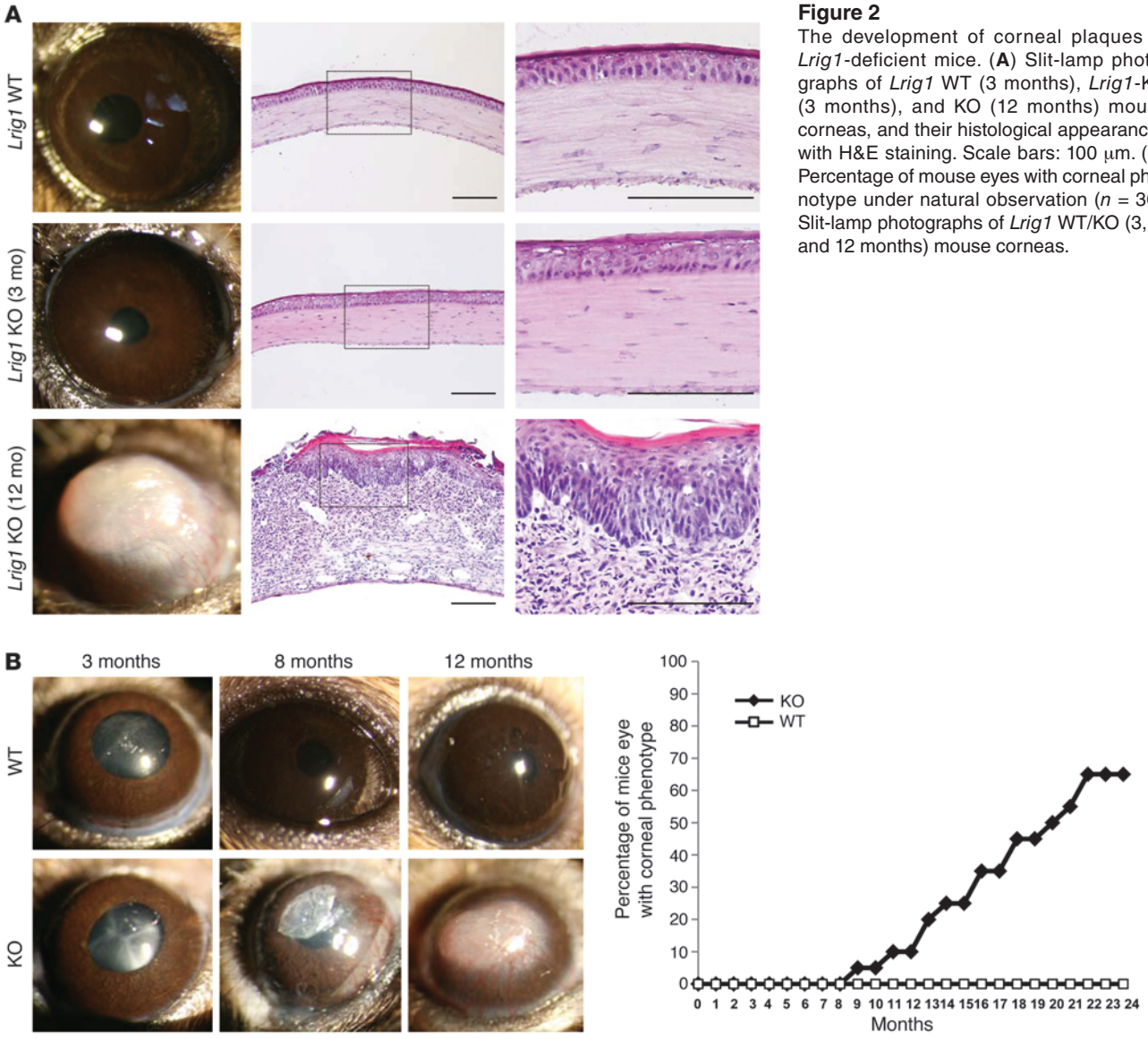

Figure 2
The development of corneal plaques in *Lrig1*-deficient mice. (**A**) Slit-lamp photographs of *Lrig1* WT (3 months), *Lrig1*-KO (3 months), and KO (12 months) mouse corneas, and their histological appearances with H&E staining. Scale bars: 100 μm. (**B**) Percentage of mouse eyes with corneal phenotype under natural observation (n = 30). Slit-lamp photographs of *Lrig1* WT/KO (3, 8, and 12 months) mouse corneas.

delayed and incomplete wound healing in the absence of *Lrig1* (Figure 4B). This finding suggests that the loss of *Lrig1* impairs the recruitment of stem/progenitor cells after wounding.

Loss of Lrig1 causes the proinflammatory state in the cornea. Once a tissue senses invading insults, various types of innate resistance are initiated to limit the tissue damage. Inflammation is generally associated with altered cytokine and chemokine expression, and proinflammatory mediators are increased and then decayed by positive and negative feedback mechanisms (20). Surprisingly, *Lrig1*-KO corneas (2–3 months) prior to wounding tended to display elevated levels of inflammatory cytokines, even in the absence of gross morphological changes (Figure 5). After injury, the levels of cytokines regulating innate lymphoid cells (ILC) and T lymphocyte subsets, such as TH1, TH2, and TH17, tended to be higher in the KO corneas as compared with the WT corneas (Figure 5). These findings suggest that the loss of *Lrig1* confers a proinflammatory state in the cornea, thus accelerating the wound-induced inflammatory responses.

Lrig1 operates as a negative regulator of the Stat3-dependent inflammatory pathway. Chronic inflammation reportedly stimulates ErbB, Wnt, and Notch signaling proteins (14–17, 19–21). Analysis of *Lrig1*-KO and WT corneas (3 and 12 months) showed no apparent difference in these signaling pathways (Supplemental Figure 3). A subset of cytokines are reportedly involved in the progression and resolution of tissue inflammation signals via the JAK/STAT pathway (22–27). Examination of *Lrig1* WT and *Lrig1*-KO corneas (3 months) showed elevated expression levels of *Stat3* in the KO tissues (Figure 6A). Moreover, *Stat3* luciferase reporter assays, using both mouse conjunctival fibroblasts and keratinocytes, showed elevated responsiveness to IL-6 upon loss of *Lrig1* (Figure 6B). This implies that *Lrig1* affects, directly or indirectly, transcriptional activation downstream of Stat3. Next, we analyzed the expression of Stat3 and phosphorylated Stat3 (pStat3, activated) in *Lrig1* WT and *Lrig1*-KO corneas (3 months). Under normal conditions, Stat3 was detected in both WT and KO corneal epithelium, yet we did not detect pStat3 (Figure 6C). Three weeks after single wound

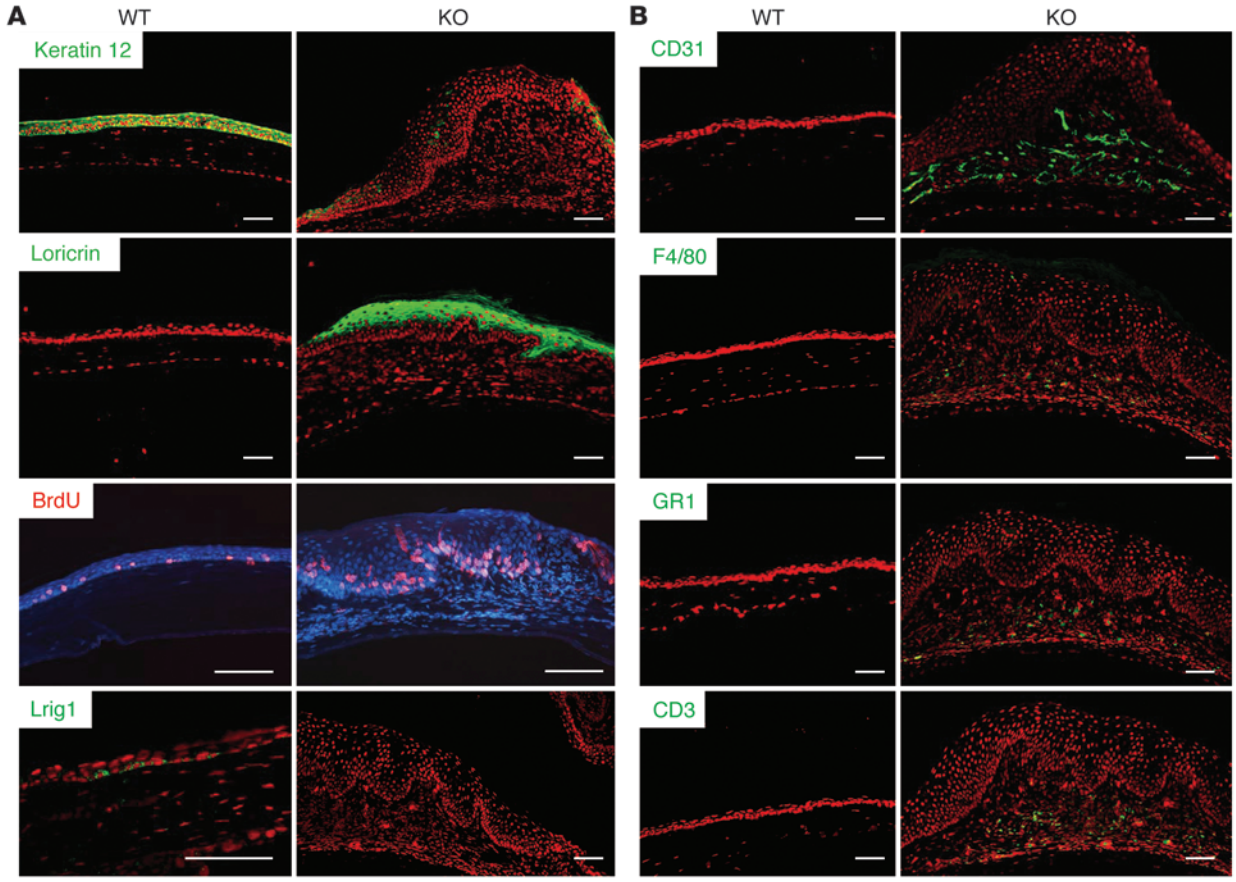

Figure 3
Cell-fate switch of the corneal epithelium resulting in the intensive infiltration of BM-derived inflammatory cells in the corneas, caused by loss of *Lrig1*. (**A**) Immunostaining for keratin 12, loricrin, LRIG1 (green), and BrdU (red) in *Lrig1* WT and *Lrig1*-KO corneas (12 months). (**B**) Immunostaining for hematopoietic cell markers such as CD31, F4/80, GR1, and CD3 (green) in *Lrig1* WT and *Lrig1*-KO corneas (12 months). Nuclei are counterstained with PI (red) and DAPI (blue). Scale bars: 100 μm.

stimulation, nuclear pStat3 was readily detected only in the *Lrig1*-KO's corneal epithelium and stroma, suggesting that *Lrig1* negatively regulated the Stat3 activation (Figure 6C). SOCS proteins are critical negative feedback regulators of the cytokine/JAK/STAT pathway and represent early processors of STAT signaling (28–30). The expression of *gp130* was unchanged in the WT and KO corneas (3 months), but RNA expression of *SOCS3* tended to be elevated in the *Lrig1*-KO tissues, both during steady-state homeostasis and upon wounding, in line with the increased STAT signaling (Figure 6D). In striking contrast, the expression of *JAK1/2* tended to be downregulated in *Lrig1*-KO corneas with wound stimulation (Figure 6D). This strongly implies that *Lrig1* operates as a negative regulator of the Stat3-dependent inflammatory pathway.

Activation of Stat3 represents the pathological phenotypes evident in Lrig1-KO corneas. In order to reveal whether epithelial activation of Stat3 sufficiently mimics the loss-in-function observed in the *Lrig1*-KO cornea, we examined the tissues from a Tg mouse model (6 months); these tissues express constitutively active *Stat3* (*K5 Stat3* Tg) in the basal layer of the epithelium (26). It is noteworthy that the Tg mice developed corneal plaques with neovascularization that, phenotypically, closely resembled that in the *Lrig1*-KO cornea (Figure 7A). Histological examination revealed pathological keratinization of the corneal epithelium, with extensive remodeling of the underlying stroma showing F4/80^{+ve} and CD3^{+ve} inflammatory infiltrates (Figure 7, B and C). This finding is also associated with cell-fate switching from keratin 12 to loricrin expression (Figure 7C), and demonstrates that activation of *Stat3* recapitulates the pathological phenotypes evident in *Lrig1*-KO corneas.

This prompted us to investigate whether Stat3 blocking would inhibit the pathological phenotypes found in *Lrig1*-KO corneas. After corneal wounding, a Stat3 inhibitor, STA21 (31, 32), was topically applied on the corneal surface 4 times a day. Seven days after wounding (7 d), WT and *Lrig1*-KO corneas (3 months) that received STA21 exhibited transparent corneas without inflammation, whereas *Lrig1*-KO corneas without STA21 exhibited corneal opacity (Figure 7D). Seven days after a second wound (14 d), WT corneas without STA21 still maintained transparency; however, *Lrig1*-KO corneas without STA21 exhibited corneal plaques with intensive inflammation and sometimes hypopyon (Figure 7, E and F). Together, these findings demonstrate that blocking Stat3 rescued the incidence of pathological phenotypes observed in the *Lrig1*-KO corneas.

Lrig1 coordinates BM-derived inflammatory cells. The intensive infiltration of inflammatory cells into the *Lrig1*-KO cornea suggests the possibility that *Lrig1* may play a critical role in stem cell–related

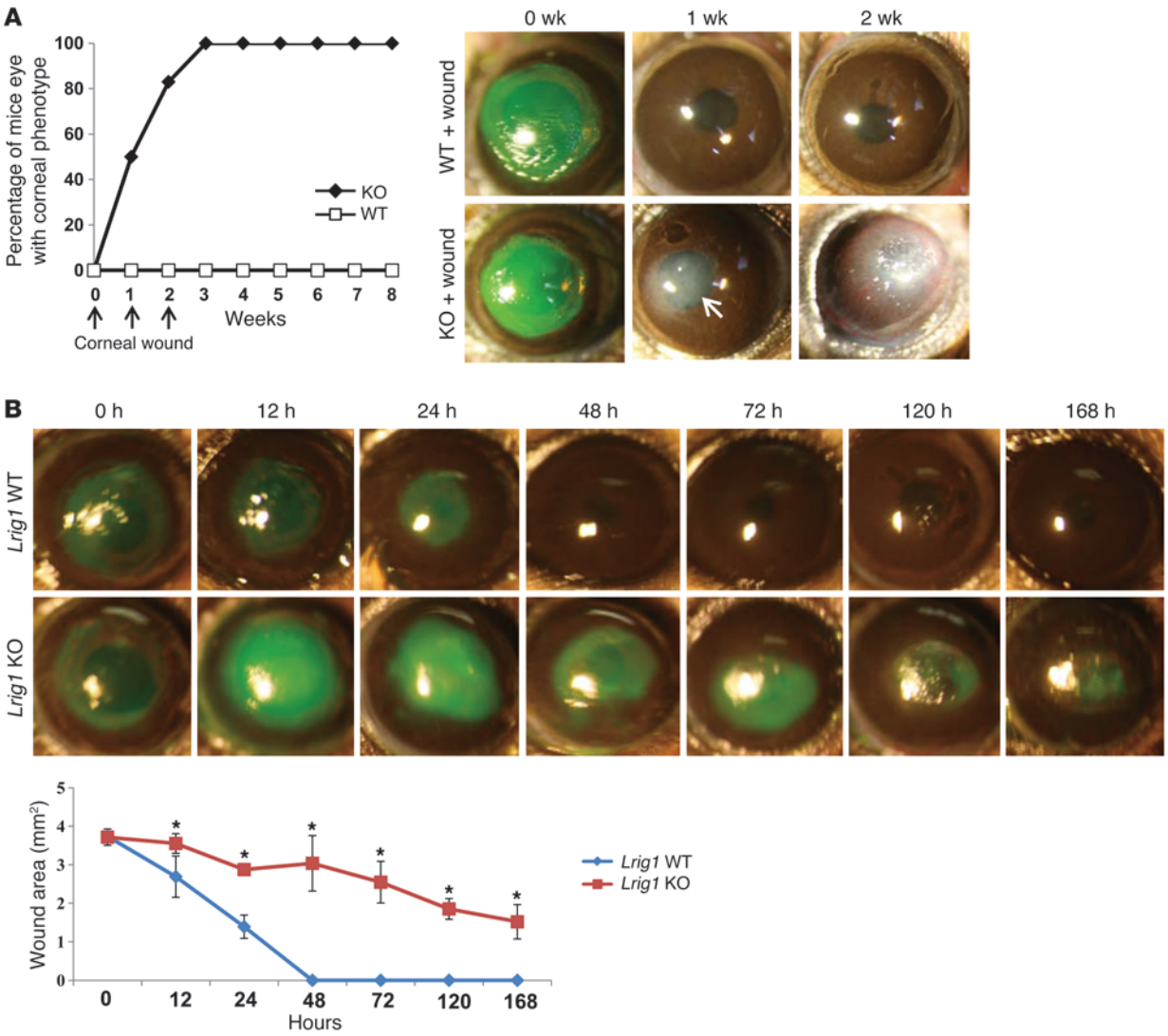

Figure 4

Wound-induced corneal stem cell replacement impaired by the loss of *Lrig1*. (**A**) Percentage of mouse eyes with corneal phenotype under wound stimulations ($n = 6$). Slit-lamp photographs of *Lrig1* WT and *Lrig1*-KO wounded corneas (3 months old) at each time point (0, 1, and 2 weeks after wounding). Fluorescein green staining was used to identify the area of epithelial defect. Corneal inflammation and subsequent corneal opacity (arrow). (**B**) Slit-lamp photographs of *Lrig1* WT and *Lrig1*-KO wounded corneas (3 months old) at each time point (0, 12, 24, 48, 72, 120, and 168 hours after wounding). Fluorescein green staining was used to identify the area of remaining epithelial defect. $^*P < 0.01$ ($n = 4$).

tissue repair in the corneal epithelium. To demonstrate the contribution of BM-derived cells in the role of LRIG1, we performed the corneal wound experiment twice (days 0 and 7) in BM chimeric mice. Validation of BM reconstitution revealed a successful hematopoietic reconstitution of primary and secondary lymphoid organs, with myeloid and lymphoid cells in all BM chimeras (Supplemental Figure 4). Before wounding (10 weeks after BM transplantation [BMT]), no mice (WT or KO) showed the abnormal corneal phenotypes. Seven days after wounding, WT (donor)→WT (recipient) mice, and KO→WT mice showed transparent corneas and no abnormal corneal phenotypes, suggesting that only KO-derived BM cells were not enough to induce the corneal phenotype (Figure 8, A–C). As expected, KO→KO mice showed corneal plaque, but cell infiltration and inflammation in the WT→KO mice was reduced (Figure 8, A and B). KO→KO mice exhibited corneal plaque with inflammatory features 21 days after wounding. However, in WT→KO mice, inflammatory features and the formation of corneal plaques were reduced, as observed both macroscopically and histologically, suggesting that WT-derived BM cells could rescue the corneal pathological phenotypes in *Lrig1*-KO corneas and that both corneal and BM cell abnormalities are needed to trigger LRIG1 pathogenesis (Figure 8, C and D). These results imply that *Lrig1* may coordinate, albeit in part, BM-derived inflammatory cells, which are essential for corneal maintenance during wound healing.

Discussion

The results of this study demonstrate that loss of *Lrig1* during corneal repair resulted in the cell-fate switch from transparent

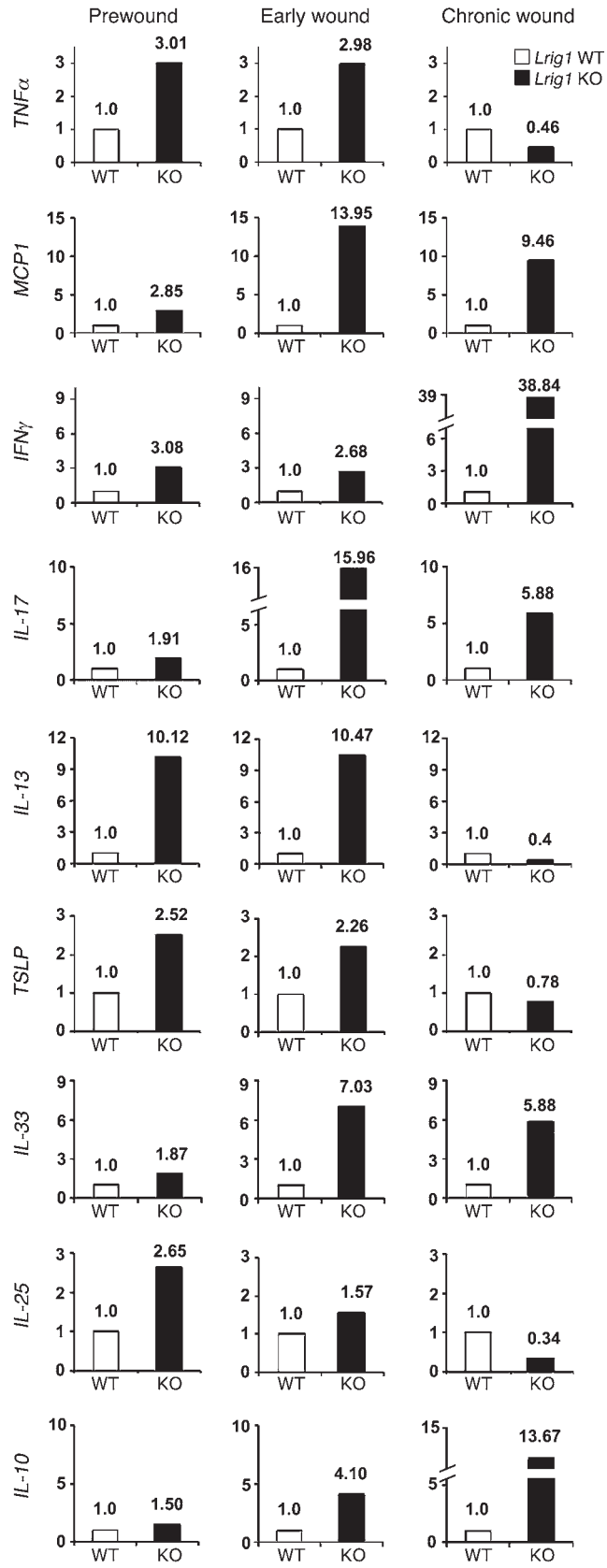

Figure 5
Loss of *Lrig1* causes the proinflammatory state in the cornea. Cytokine profiles (*TNFα*, *MCP1*, *IFNγ*, *TSLP*, and *IL-5/10/13/17/25/33*) of *Lrig1* WT and *Lrig1*-KO corneas (2–3 months) in the prewound, early wound, and chronic wound stage by real-time PCR (n = 4 corneas mixed). Numbers show relative mRNA expression.

corneal epithelium to keratinized skin-like epidermis, leading to corneal blindness. This pathological skin-like epithelium differed from the physiological mouse epidermis, as it showed epithelial hyperproliferation and invaginations into the underlying corneal stroma. A previous report indicated that LRIG1 expression defines a distinct multipotent stem cell population in mammalian epidermis and normally contributes to the interfollicular epidermis and sebaceous glands (15). Our findings show that *Lrig1*-KO corneas with wounding formed corneal plaques with massive neovascularization and intense infiltration of inflammatory cells. However, the findings of a previous report from a member of our group illustrated that *Lrig1*-KO mice, with or without minor wound stimulation on the trunk skin, did not develop any epidermal hyperplasia (psoriasiform skin changes), suggesting that more continuous wounding might be needed to induce the phenotypes in the areas covered with thick hair (13).

In a normal situation, tear film is essential for maintaining the stability of ocular surface epithelium; therefore, eyelids, including meibomian glands, have a critical role in corneal homeostasis. The other findings of a previous report from a member of our group demonstrated that Notch1 deficiency results in loss of meibomian glands, causing the loss of tear film, and microlesions of the corneal epithelium (19). We thus examined the morphology of eyelids in *Lrig1*-KO mice and found that there were no abnormal phenotypes in them (data not shown). Further investigation regarding Notch1 and LRIG1 interaction is needed to clarify this point.

In our observation series, *Lrig1*-KO corneas gradually formed corneal plaques and, finally, approximately 70% of the *Lrig1*-KO mice developed abnormal corneal phenotypes within 24 months. Although we breed the mice under specific pathogen–free conditions and we only observed the corneal phenotype in *Lrig1*-KO mice, not in the WT mice, caged mice often receive repeated small wounds to the epithelial surface and it seems highly likely that these events might precipitate the phenotype in older mice.

One of the most striking findings is that the loss of *Lrig1* confers a proinflammatory state in the cornea, and after wound stimulation, *Lrig1*-KO corneas exhibited extensive cellular infiltration and inflammation. The cornea is a unique transparent epithelial tissue in the body, and nature has found a way to provide the cornea with an antiinflammatory system that greatly reduces the threat of inflammation-induced visual loss (6). Tissue-intrinsic inflammatory responses recruit hematopoietic cells that amplify the response through their innate receptors, triggered by endogenous ligands present in the inflamed tissue. Thus, the remodeling of corneal stroma was characterized by the existence of blood vessels (neovascularization), infiltration of inflammatory cells, morphological changes of collagen fibrils, and abnormal corneal keratocytes (Supplemental Figure 5). Immunohistochemistry revealed that hematopoietic cell markers were distinctly expressed in the remodeling stroma of the *Lrig1*-KO corneas, whereas no or limited expression was observed in the *Lrig1* WT corneas. In view of these findings, it is clear that

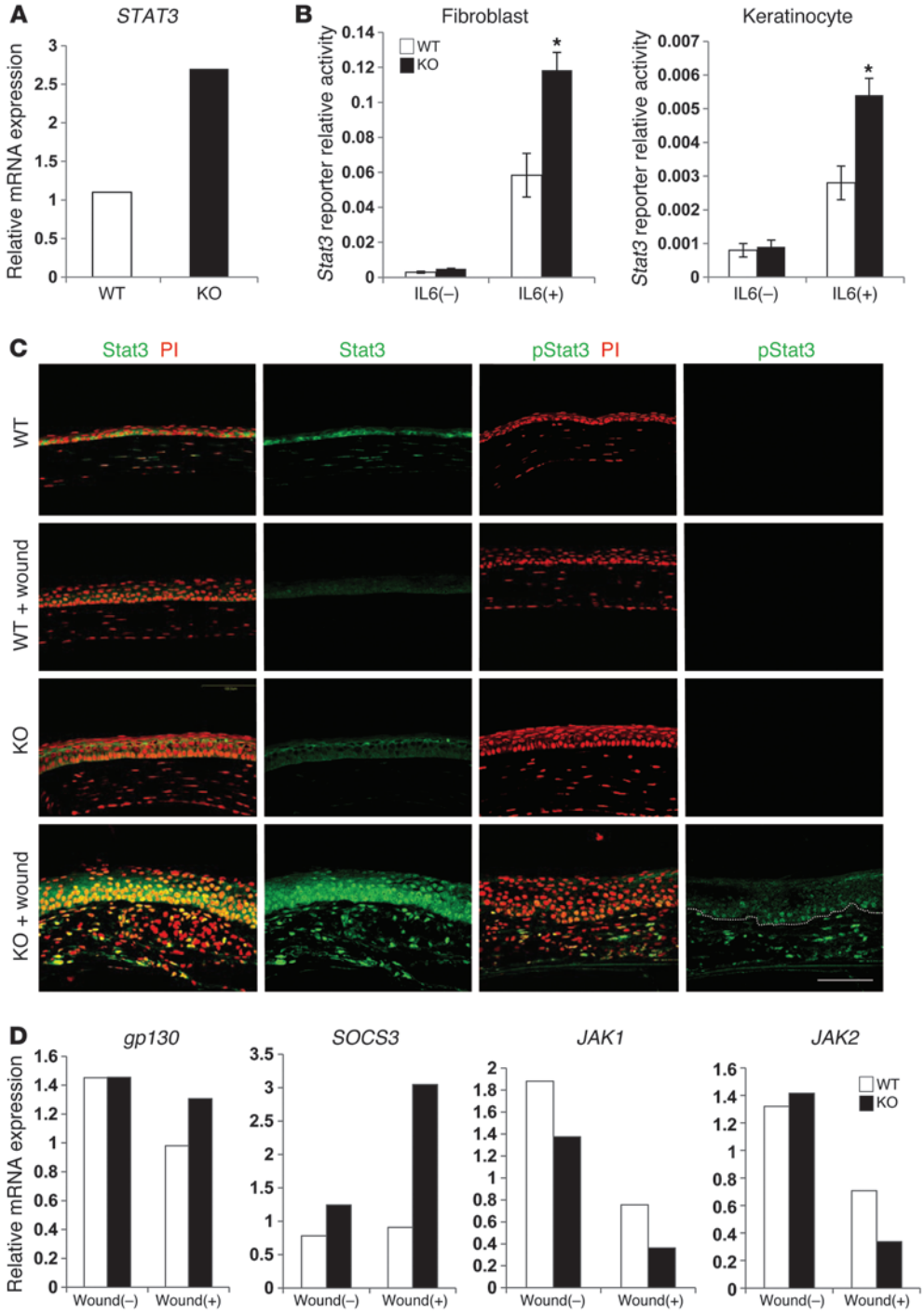

Figure 6
Stat3 activation induced by the loss of *Lrig1*. (**A**) Relative expression of *Stat3* in *Lrig1* WT and *Lrig1*-KO corneas (n = 4 corneas mixed, 3 months). (**B**) *Stat3* expression transcriptionally inhibited by *Lrig1*. Luciferase reporter assay using mouse cultured conjunctival fibroblast and keratinocytes, with or without IL-6 stimulation. *$P < 0.01$ (n = 4). (**C**) Immunohistochemistry for Stat3 and pStat3 (green) in *Lrig1* WT and *Lrig1*-KO corneas (3 months), with or without wound. Nuclei are counterstained with PI (red). Dashed lines indicate the border between epithelium and underlying stroma. Scale bar: 100 μm. (**D**) Relative expression of JAK/STAT-related molecules (*gp130*, *SOCS3*, and *JAK1* and *JAK2*) in *Lrig1* WT and *Lrig1*-KO corneas, with or without wound (n = 4 corneas mixed, 3 months).

LRIG1 modulates the ocular antiinflammatory system and may have some role in maintaining corneal transparency.

It has been reported that cell-fate decision depends on the surrounding microenvironment (niche) and that stem cells and niche cells exchange specific signals with one another (7, 8). Interestingly, development of corneal plaques in *Lrig1*-KO mice was always accompanied by the remodeling of the corneal stroma. The kinetic study revealed that cell-fate changes in the *Lrig1*-KO cornea were preceded by changes within the underlying corneal stroma. The loss of *Lrig1* in the corneal epithelium resulted first in the upregulation of various kinds of cytokines regulating ILC and T cell subsets. Subsequently, they recruited inflammation-inducible hematopoietic cells to the cornea, finally leading to the remodeling of the corneal stroma. Only after formation of this microenvironment did the *Lrig1*-KO corneal cells undergo the phenotype switch. These findings suggest that the microenvironment must provide tissue-specific signals that allow corneal epithelial cells to change their phenotypes. The mechanism of the cell-fate switch

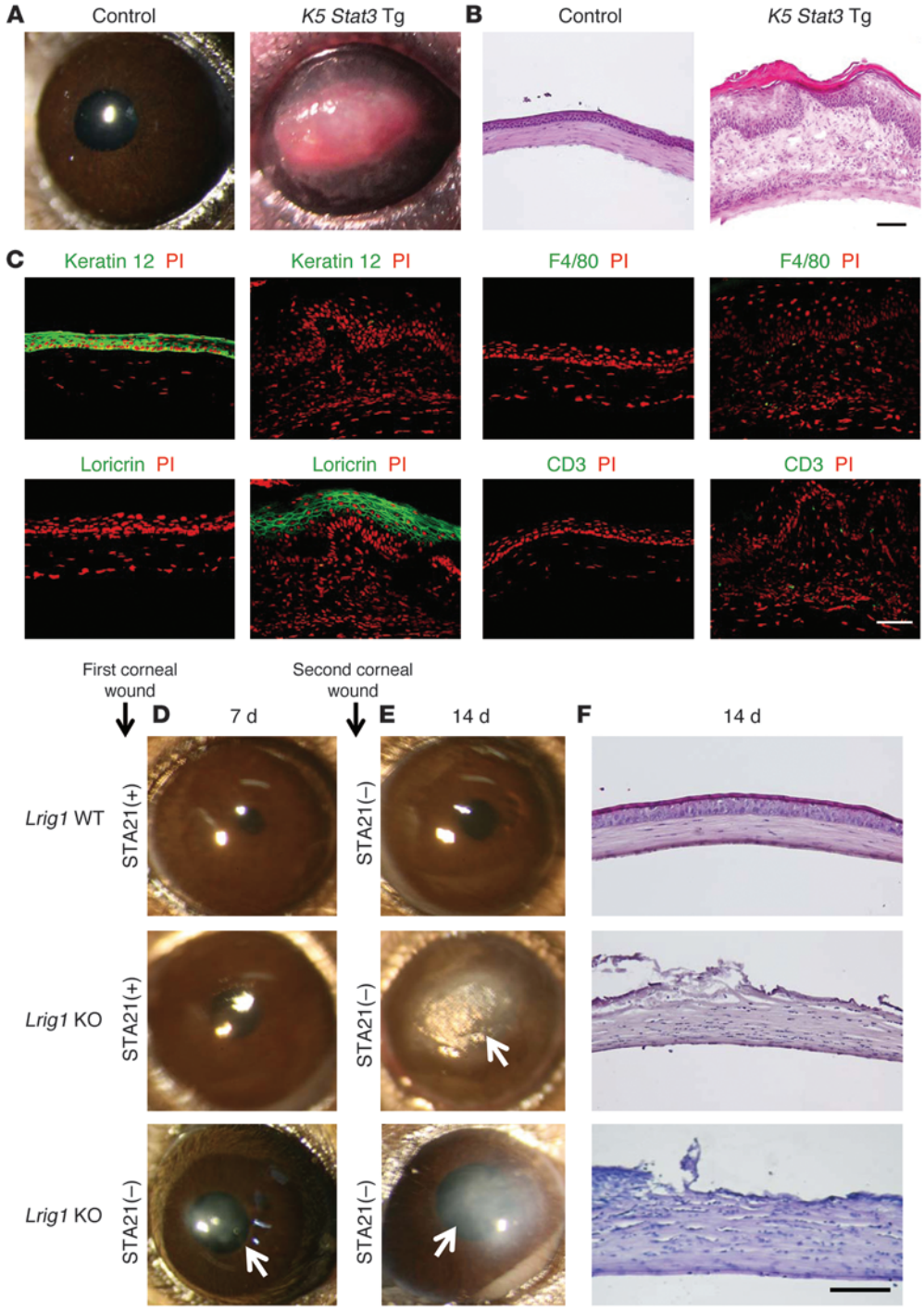

Figure 7
Reproduction of pathological phenotypes evident in *Lrig1*-KO corneas resulting from the activation of *Stat3*. (**A** and **B**) Slit-lamp photographs and histological appearances with H&E staining of control and *K5 Stat3* Tg mouse corneas (6 months). Scale bars: 100 μm. (**C**) Immunohistochemistry for keratin 12, loricrin, F4/80, and CD3 (green) in control and *K5 Stat3* Tg corneas. Nuclei are counterstained with PI (red). Scale bar: 100 μm. Generation of *Lrig1*-KO corneal phenotypes rescued by blocking Stat3. (**D**) Seven days after the first corneal wound (7 d), *Lrig1* WT and *Lrig1*-KO corneas (3 months) treated with STA21 were transparent, without inflammation, yet *Lrig1*-KO corneas without STA21 showed corneal opacity (arrow). (**E**) Seven days after the second wound (14 d), *Lrig1* WT corneas without STA21 still maintained their transparency, while *Lrig1*-KO corneas without STA21 exhibited corneal plaques with inflammation (arrows). (**F**) Histological appearances of the resultant corneas (14 d) with H&E staining. Scale bar: 100 μm.

of the *Lrig1*-KO cornea after wounding seems to be the result of tissue-intrinsic inflammatory responses.

In chronically inflamed murine tissues, several factors, including NF-κB, TGF-β1, bone morphogenetic proteins, and Wnt, Notch, and ErbB signaling proteins, are upregulated in the context of inflammation, thus leading to mesenchymal differentiation and a strong inductive signal for stem-cell proliferation (14–17, 19–21). In *Lrig1*-KO corneas, we were unable to confirm any distinction in the expression of these factors from those in the WT corneas. Various cytokines are involved in the progression and resolution of tissue inflammation, and most cytokines utilize the so-called JAK/STAT pathway (22–27). Therefore, we next focused on the JAK/STAT pathway as a potential target for further investigations.

STATs are a family of latent cytoplasmic proteins involved in transmitting extracellular signals to the nucleus (22–24). Most surprisingly, continuous activation of Stat3 resulted in the reproduction of pathological phenotypes evident in *Lrig1*-KO corneas. Stat3 reportedly plays a critical role in various biological activities,

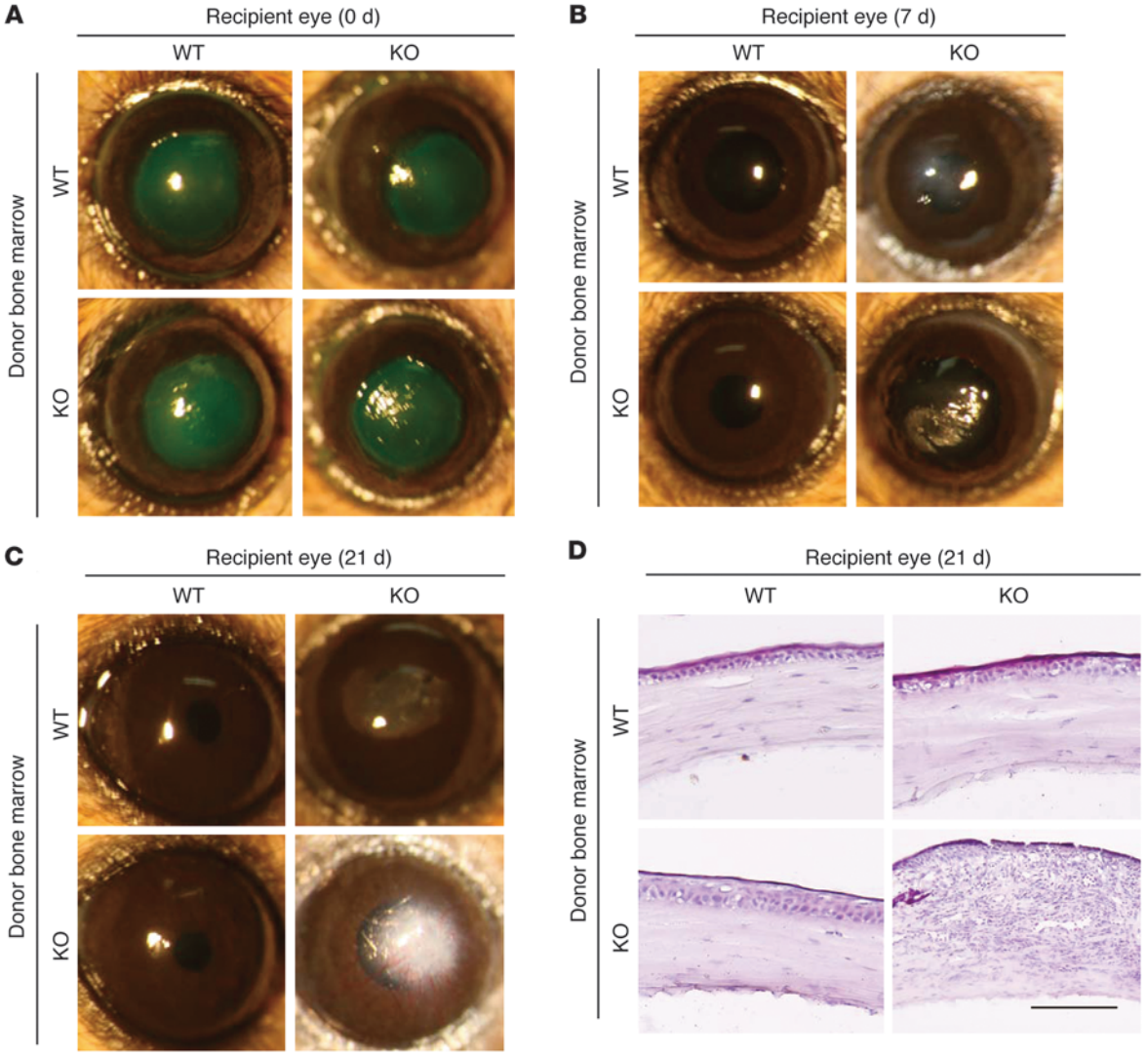

Figure 8
The corneal pathological phenotypes in *Lrig1*-KO mice rescued by WT-derived BM cells. (**A**–**C**) Slit-lamp photographs of BM chimera mice corneas at each time point (0, 7, and 21 days after wounding, n = 4 or 5). Fluorescein green staining was used to identify the area of remaining epithelial defect. (**D**) Histological appearances with H&E staining of BM chimera mouse corneas. Scale bar: 100 μm.

including cell proliferation, survival, and migration. Sano et al. previously reported that Stat3 is activated in keratinocytes of human psoriatic lesions, and Tg mice expressing a constitutively active form of *Stat3* in keratinocytes developed skin lesions, either spontaneously or in response to wounding, that closely resemble human psoriasis (26). Itami et al. also reported that loss of *Lrig1* resulted in psoriasiform epidermal hyperplasia and that LRIG1 expression was apparently downregulated in human psoriatic lesions (13). Using a mouse model, we clearly demonstrate that activation of *Stat3* reproduced the pathological phenotypes observed in *Lrig1*-KO corneas and abrogation of Stat3 function inhibited the corneal phenotype switch, thus suggesting that LRIG1 and Stat3 molecules are closely linked with one another, both clinically and biologically. In addition, we have performed immunohistochemistry for pStat3 in pathologically keratinized corneal tissues in patients with severe ocular surface disease and have found that pStat3 was sporadically expressed in them (data not shown). Thus, we presume that Stat3 inhibitor–based therapy might be effective for treating patients with most severe ocular surface diseases.

We demonstrated the interaction between LRIG1 and the Stat3 molecule, but its precise mechanism has yet to be determined. It has been reported that LRIG1 is a negative regulator of EGF and Met receptors and that LRIG1-mediated receptor ubiquitination and degradation may contribute to the suppression of these receptor functions (33–35). In view of these previous findings, it could also be possible that LRIG1 regulates the expression of these receptors, thereby limiting their activities. From our experiments, we only demonstrated that LRIG1, directly or indirectly, regulates Stat3 activation. Future extensive study is needed to clarify this point.

Tissue-intrinsic inflammatory responses recruit hematopoietic cells, and characterization of the inflammatory infiltrates in remodeling *Lrig1*-KO tissues obviously showed pronounced recruit-

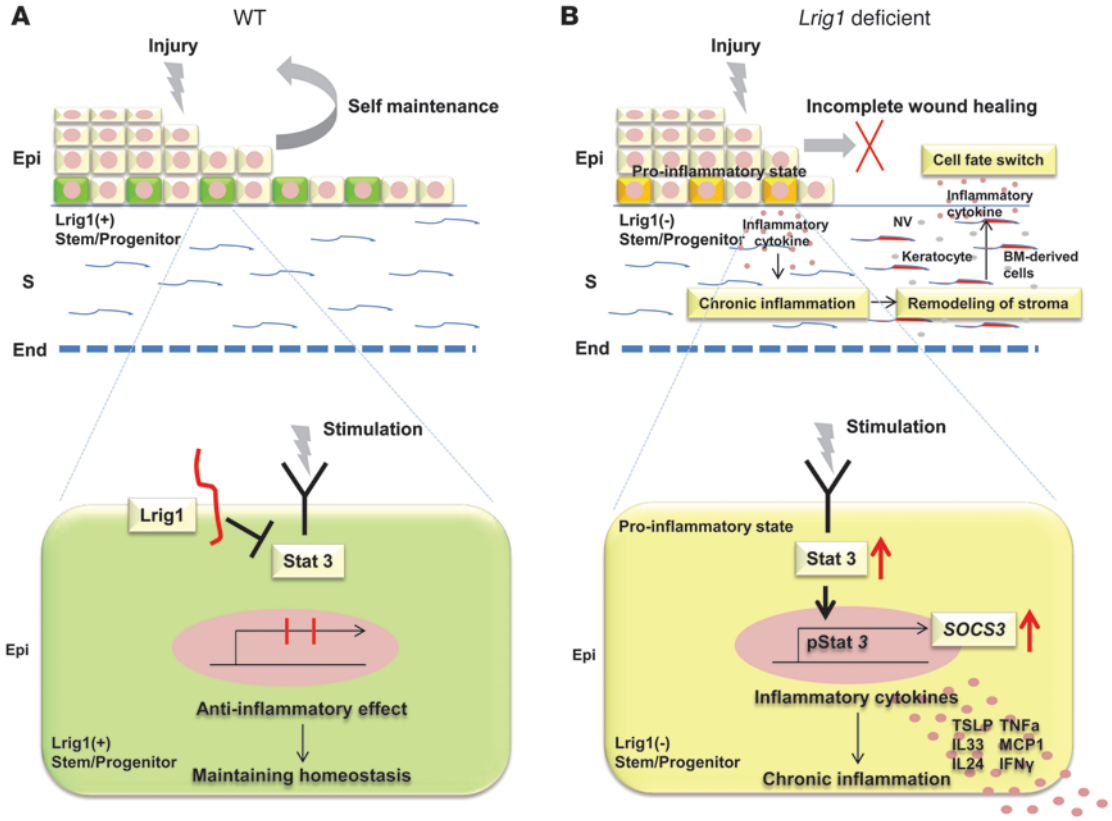

Figure 9

Model of the function of LRIG1 in corneal homeostasis. (**A**) In a normal situation (WT), the cornea is self-renewed by *Lrig1*(+) corneal stem/progenitor cells after injury. Corneal transparency is maintained via negative regulation of the Stat3-dependent inflammatory pathway by LRIG1. (**B**) Loss of *Lrig1* (KO) causes the proinflammatory state in *Lrig1* (–) corneal stem/progenitor cells, and impairs wound-induced stem cell replacement (delayed/incomplete wound healing). Loss of *Lrig1* activates the Stat3-dependent inflammatory pathway and induces chronic inflammation, resulting in remodeling of the corneal stroma. Inductive BM-derived cells secrete inflammatory cytokines and cause the cell-fate changes to keratinized epithelium. Epi, corneal epithelium; S, corneal stroma; End, corneal endothelium; NV, neovascularization.

ment of CD31-, F4/80-, GR1-, and CD3-positive cells, suggesting that LRIG1 might coordinate BM-derived inflammatory cell behavior. In fact, Sano et al. previously showed a dual requirement for activated *Stat3* in epidermal keratinocytes as well as activated T lymphocytes in the skin of Tg mice for development of psoriatic lesions, leading to the hypothesis that the changes in *Stat3*-regulated genes in keratinocytes cooperate with activated immunocytes in the development of psoriasis (26). BM-derived cells are credited with playing a critical role in the resolution of inflammation and tissue repair, not just under homeostatic conditions, but also as key players in tissue repair during wound healing through the interplay with cells bearing stem or progenitor cell properties.

Scientifically, it is extremely important to find the corneal disease model linked to LRIG1. In fact, we demonstrated the activation of Stat3 in pathologically keratinized epithelium in severe ocular surface diseases, yet we have thus far found no direct evidence of corneal disease linked to LRIG1. However, we did find that the abnormal corneal epithelial differentiation (malignancy) leads to the loss of *Lrig1* in squamous cell carcinomas of the ocular surface epithelium (data not shown). The relationship between tumorigenesis and the stem cell–related inflammatory pathway is difficult to elucidate, and future extensive examination is needed to clarify this point.

Previous biological findings showed that LRIG1 controls the fundamental signal network within the epithelial area (13–17), and there are no reports to date that demonstrate the crosstalk between the epithelium and the surrounding microenvironment. The cellular microenvironment is crucial for the maintenance of stem cells as well as for cell-fate decision during tissue repair. BM-derived cells reportedly stabilize their surrounding tissue microenvironments by adapting different phenotypes as feed-forward mechanisms to maintain tissue homeostasis (36–42). Based on the results of our corneal wound experiment using BM chimera mice, we hypothesize that LRIG1 might regulate BM-derived cell behavior. However, its precise mechanism is a complex organismal process and remains to be determined.

Importantly, and based on the findings in the present study, ocular inflammation is incompatible with good vision, and corneal cell fate during repair is not only maintained by corneal epithelial stem cells, but also by BM-derived inflammatory cells, whose functions are well controlled by the Lrig1/Stat3 inflammatory pathway (Figure 9). In view of these and previous findings on the function of LRIG1 in epidermal and intestinal stem cells (13–17), we theorize that LRIG1 provides a general mechanism to control systemic tissue homeostasis and serves as a target for therapeutic exploitation.

Methods

Mice. *Lrig1*-KO mice were regenerated from cryopreserved sperm (C57BL/6 background) (13). Genotyping was performed using 3 different primers (Supplemental Table 2; WT: 322 bp, KO: 400 bp). The *K5 Stat3* Tg mice were as described previously (26). Mice were born with the expected ratio of Mendelian inheritance, and no changes in sex ratios were observed.

Tissues. All human cornea tissues were obtained from SightLife Eye Bank, and all corneas were stored at 4°C in storage medium (Optisol-GS; Bausch & Lomb).

Antibodies. For immunohistochemistry, the following antibodies were used: mouse mAb anti–β-catenin (610153, ×200; BD Biosciences), rat mAbs anti-BrdU (ab6326, ×200; Abcam Plc), anti-CD31 (550274, ×200; BD Biosciences), anti-F4/80 (RM2900, ×100; Life Technologies), anti-GR1 (553128, ×100; BD Biosciences), and anti-CD3 (MAB4841, ×100; R&D Systems, Inc.), rabbit polyclonal antibodies (pAbs) anti-LRIG1 (×200; provided by S. Itami, Osaka University), anti-loricrin (PRB-145P, ×700; COVANCE), anti–keratin 12 (KR074, ×200; Transgenic), anti-Stat3 (9132, ×200; Cell Signaling Technology), anti–phospho-Stat3 (9131, ×200; Cell Signaling Technology), anti–phospho-EGFR (ab40815, ×200; Abcam), and anti–c-Met (sc-162, ×50; Santa Cruz Biotechnology, Inc.), goat pAbs anti-LRIG1 (sc-50076, ×200; Santa Cruz Biotechnology), anti-EGFR (E1282, ×100; Sigma-Aldrich), and anti-Notch1 (sc-6014, ×50; Santa Cruz Biotechnology Inc.). Secondary antibodies included Alexa Fluor 488 anti-mouse, rat, rabbit, and goat IgG (×1500), and Alexa Fluor 594 anti-rat IgG (×1500) (Molecular Probes). Antibodies used for cell surface staining were phycoerythrin-conjugated αCD8 (53-6.7), fluorescein isothiocyanate–conjugated αF4/80 (BM8) and αCD4 (RM4-5), allophycocyanin-conjugated αCD19 (1D3), PeCy7-conjugated αIgM (II/41), and αCD11b (M1/70) (eBioscience Inc.).

Clonal analysis. For clonal analysis, we applied the method of Barrandon and Green (11). Secondary cultures of human corneal epithelial cells were used. Briefly, single cells isolated under an inverted microscope were inoculated into 12-well plates that contained a feeder layer of mitomycin C–inactivated NIH-3T3 fibroblasts. After 7 days, a single clone was identified under an inverted microscope and then photographed. Each clone was then divided into 2 parts; 3/4 of the clone was used for DNA chip assay, and the other 1/4 of the clone was transferred to an indicator dish, fixed 10 to 12 days later, and stained with 0.1% toluidine blue for classification of the clonal type, which was determined by the percentage of aborted colonies (11, 43). When 0% to 5% of the colonies became terminal, the clone was classified as a holoclone. When all colonies were terminal or when no colonies formed, the clone was classified as a paraclone.

Gene expression analysis. Gene expression profiles were examined by use of a high-density oligonucleotide probe array, GeneChip, of Human Genome U133 Plus 2.0 (Affymetrix). Total RNA was extracted using the RNeasy kit (QIAGEN). cRNA preparation and target hybridization were performed according to the Affymetrix GeneChip technical protocol. The DNA chips were scanned with a specially designed confocal scanner (GeneChip Scanner 3000; Affymetrix). Array data analysis was performed with Affymetrix GeneChip Operating Software (GCOS) version 1.0. The full list of normalized human DNA chip data is presented in Supplemental Table 2.

Immunohistochemistry. Immunohistochemical studies followed our previously described method (43, 44). Briefly, 8-μm–thick sections were placed on silane-coated slides, air dried, and then fixed in 100% acetone or 4% paraformaldehyde at 4°C for 15 minutes. After washing in PBS at room temperature (RT) for 15 minutes, sections were incubated with 1% BSA (Sigma-Aldrich Corporation) at RT for 30 minutes to block nonspecific binding. Sections were then incubated with primary antibody at RT for 1 hour and washed 3 times in PBS containing 0.15% TRITON X-100 (Dow Chemical Company) for 15 minutes. Control incubations were with the appropriate normal mouse, rat, rabbit, and goat IgG at the same concentration as the primary antibody, and the primary antibody for the respective specimen was omitted. The sections were then incubated with appropriate secondary antibodies at RT for 1 hour. After being washed 3 times with PBS, the sections were then mounted using glycerol containing propidium iodide (PI) or DAPI (Vectashield; Vector Laboratories Inc.), and examined under a confocal microscope (Fluoview; Olympus Corp.).

Electron microscopy. Following our previous protocol (45), whole eyes were examined by transmission electron microscopy (TEM). Specimens were fixed in 2.5% glutaraldehyde in 0.1 M PBS, washed 3 times for 15 minutes in PBS, and post-fixed for 2 hours in 2% aqueous osmium tetroxide. They were then washed 3 more times in PBS before being passed through a graded ethanol series. For TEM preparation, the specimens were embedded in Agar 100-epoxy resin (Agar Scientific). Ultrathin (70 nm) sections were collected on copper grids and stained for 1 hour each with uranyl acetate and 1% phosphotungstic acid, and then for 20 minutes with Reynold's lead citrate prior to examination on a transmission electron microscope (JEM 1010; JEOL Ltd.).

Real-time PCR. Since the mouse cornea is very small, we optimized the conditions to improve the quality and accuracy of this experiment. We found that pooling 4 corneas was the minimum required to perform quantitative PCRs. The efficacy of each primer set used was also checked before the experiments were performed. All samples were homogenized in RLT lysis buffer (QIAGEN), and total RNA was eluted using the RNeasy Mini Kit (QIAGEN) according to the manufacturer's recommendations. After reverse transcription and cDNA synthesis, the relative abundance of transcripts was detected by SYBR Green PCR Master Mix (Applied Biosystems) according to the manufacturer's instructions. The average value of duplicates from each transcript was used for comparison, and the expression levels of the individual transcripts were normalized by the expression level of β-actin. The primers that were used are shown in Supplemental Table 3.

BrdU labeling. According to the manufacturer's protocol (Zymed Laboratories Inc.), we injected the *Lrig1* mice ($n = 3$) and cultured corneal epithelial cells on amniotic membrane with BrdU-labeling reagent (1 ml/100 g). After 2 hours, the mice were sacrificed, and the eye and cultured cells were then embedded in Tissue-Tek II OCT compound (Sakura Finetek Europe B.V.).

3D culture. Mouse corneal epithelial cells were cultured according to our previously reported system (43–46). Corneal epithelial explants, including the corneal limbus ($n = 3$), were put onto denuded amniotic membrane substrate spread on the bottom of culture inserts and cocultured for 14 days with mitomycin C–inactivated 3T3 fibroblasts (2×10^4 cells/cm^2). The culture medium consisted of a defined keratinocyte growth medium (KGM) (Gibco; Life Technologies) supplemented with 5% FBS. The cultures were incubated at 37°C in a 5% CO_2–95% air incubator, and the medium was changed daily.

In vivo wound model. Experimental mice (*Lrig1* WT and *Lrig1*-KO, 8 weeks old, $n = 4$ each) were anesthetized by intraperitoneal injection of combined xylazine and ketamine. After an administration of topical oxybuprocaine eye drops (Santen Pharmaceutical Co.), central corneal epithelial debridement was performed, using a commercially available hand-held diamond-tipped glass engraver (IH-640; Ito Co.), under a stereomicroscope. Briefly, we used a 2-mm trephine to demarcate the margins of the wound (both single and repeated wounds) to avoid damaging the peripheral cornea and limbal areas. To perform the repeated wound, we first used fluorescein green staining to identify areas of intact epithelial tissue. If there was intact epithelium within the 2-mm demarked area, it was removed with the hand-held diamond-tipped glass engraver. At this point, we paid careful attention to avoid damaging the corneal stroma as much as possible. The experimental mice were killed by an overdose of sodium pentobarbital, and the eyes were then enucleated and embedded in OCT compound. To observe the area of remaining epithelial defect at the different time points, fluorescein green staining was used.

Luciferase promoter assay. Transfection of luciferase reporters into cultured *Lrig1* WT and *Lrig1*-KO mice conjunctival fibroblasts and keratinocytes followed our previous protocol (47). Both fibroblasts and keratinocytes were plated in 24-well culture plates and cultured in DMEM with 10% FBS (fibroblast) or defined KGM (keratinocyte) for 18 to 24 hours before transfection. A *Stat3* Reporter Assay Kit (QIAGEN) was used to measure the transcription factor activity. Cells (3×10^4) were cotransfected by Lipofectamine (fibroblast; Life Technologies) or FuGENE HD (keratinocyte; Promega) for 24 hours, followed by cytokine treatment (IL-6; BioLegend Inc.) for 6 hours. The resultant cells were lysed with 100 μl Passive Lysis Buffer (Promega). Luciferase activity was read on a Veritas Microplate Luminometer (Promega).

Generation of BM chimera mice. BM chimera mice were generated with 5×10^6 freshly isolated total BM cells from the femur and tibia of *Lrig1* WT or *Lrig1*-KO mice (donor, 10–12 weeks), respectively, following our previous protocol (48, 49). Isolated cells were intravenously injected either into lethally irradiated (900 cGY) *Lrig1* WT or *Lrig1*-KO mice (host, 16–18 weeks). A mechanical corneal wound was applied to the hosts 10 weeks after BM reconstitution. The efficiency of corneal wound healing and hematopoietic reconstitution of lymphoid organs of the hosts by donor-derived cells was assessed 13 weeks after BM transfer by genotyping tail, thymus, and BM DNA. Furthermore, lymphoid organs of reconstituted mice were analyzed by FACS as described below and were compared in statistical analysis to those of age-matched *Lrig1* WT or *Lrig1*-KO mice.

Flow cytometric analysis. Single-cell suspensions of freshly isolated thymus, spleen, and total BM cells of the femur and tibia were subsequently incubated with αCD16/CD32 for 10 minutes, followed by staining with a combination of conjugated antibodies in FACS buffer (PBS + 4% heat-inactivated FCS + 2 mM EDTA) for 30 minutes. Stained cells were analyzed on a FACSCanto II flow cytometer (BD Biosciences).

Statistics. The 2-tailed, unpaired Student's *t* test was used to compare the differences between 2 groups, and *P* values of less than 0.05 or less than 0.01 were considered significant. The values are presented as mean ± SD. FACS data were analyzed with FlowJo software (TreeStar Inc.) and GraphPad Prism software (GraphPad Software Inc.). Statistical significance was determined using a 2-tailed Mann-Whitney *U* test for paired samples or 1-way ANOVA and nonparametric tests for multiple groups. $P < 0.05$ was considered statistically significant.

Study approval. All animals used for this study were maintained and handled according to the protocols approved by the Kyoto Prefectural University of Medicine. All animal studies were approved by the Committee on Animal Research of Kyoto Prefectural University of Medicine. All experiments were performed in accordance with the tenets set forth in the Declaration of Helsinki.

Acknowledgments

We especially thank Kim B. Jensen for critical comments on the manuscript. We also thank Y. Hata, H. Saito, T. Horikiri, S. Mano, and K. Yamazaki for assisting with the experimental procedures, and J. Bush and A.W. Amici for reviewing the manuscript. This study was supported in part by Grants-in-Aid for scientific research from the Japanese Ministry of Education, Culture, Sports, Science and Technology (no. 23592621), the JST-ETH Strategic Japanese-Swiss Cooperative Program (Heisei 20), the EPFL, the CHUV, OptiStem, and BBSRC (UK).

Received for publication June 11, 2013, and accepted in revised form October 3, 2013.

Address correspondence to: Takahiro Nakamura, Department of Ophthalmology, Kyoto Prefectural University of Medicine, Kawaramachi Hirokoji, Kamigyo-ku, Kyoto 602-0841, Japan. Phone: 81.75.251.5578; Fax: 81.75.251.5663; E-mail: tnakamur@koto.kpu-m.ac.jp.

1. Whitche JP, Srinivasan M, Upadhyay MP. Corneal blindness: a global perspective. *Bull World Health Organ*. 2001;79(3):214–221.
2. Lavker RM, Sun TT. Epithelial stem cells: the eye provides a vision. *Eye (Lond)*. 2003;17(8):937–942.
3. De Luca M, Pellegrini G, Green H. Regeneration of squamous epithelia from stem cells of cultured grafts. *Regen Med*. 2006;1(1):45–57.
4. Rama P, Matuska S, Paganoni G, Spinelli A, De Luca M, Pellegrini G. Limbal stem-cell therapy and long-term corneal regeneration. *N Engl J Med*. 2010; 363(2):147–155.
5. Tan DT, Dart JK, Holland EJ, Kinoshita S. Corneal transplantation. *Lancet*. 2012;379(9827):1749–1761.
6. Streilein JW. Ocular immune privilege: therapeutic opportunities from an experiment of nature. *Nat Rev Immunol*. 2003;3(11):879–889.
7. Blanpain C, Horsley V, Fuchs E. Epithelial stem cells: turning over new leaves. *Cell*. 2007;128(3):445–458.
8. Li L, Clevers H. Coexistence of quiescent and active adult stem cells in mammals. *Science*. 2010; 327(5965):542–545.
9. Schermer A, Galvin S, Sun TT. Differentiation-related expression of a major 64K corneal keratin in vivo and in culture suggests limbal location of corneal epithelial stem cells. *J Cell Biol*. 1986;103(1):49–62.
10. Cotsarelis G, Cheng SZ, Dong G, Sun TT, Lavker RM. Existence of slow-cycling limbal epithelial basal cells that can be preferentially stimulated to proliferate: implications on epithelial stem cells. *Cell*. 1989;57(2):201–209.
11. Barrandon Y, Green H. Three clonal types of keratinocyte with different capacities for multiplication. *Proc Natl Acad Sci U S A*. 1987;84(8):2302–2306.
12. Pellegrini G, et al. Location and clonal analysis of stem cells and their differentiated progeny in the human ocular surface. *J Cell Biol*. 1999;145(4):769–782.
13. Suzuki Y, et al. Targeted disruption of LIG-1 gene results in psoriasiform epidermal hyperplasia. *FEBS Lett*. 2002;521(1–3):67–71.
14. Jensen KB, Watt FM. Single-cell expression profiling of human epidermal stem and transit-amplifying cells: Lrig1 is a regulator of stem cell quiescence. *Proc Natl Acad Sci U S A*. 2006;103(32):11958–11963.
15. Jensen KB, et al. Lrig1 expression defines a distinct multipotent stem cell population in mammalian epidermis. *Cell Stem Cell*. 2009;4(5):427–439.
16. Wong VW, et al. Lrig1 controls intestinal stem-cell homeostasis by negative regulation of ErbB signalling. *Nat Cell Biol*. 2012;14(4):401–408.
17. Powell AE, et al. The pan-ErbB negative regulator Lrig1 is an intestinal stem cell marker that functions as a tumor suppressor. *Cell*. 2012;149(1):146–158.
18. Majo F, Rochat A, Nicolas M, Jaoude GA, Barrandon Y. Oligopotent stem cells are distributed throughout the mammalian ocular surface. *Nature*. 2008;456(7219):250–254.
19. Vauclair S, Majo F, Durham AD, Ghyselinck NB, Barrandon Y, Radtke F. Corneal epithelial cell fate is maintained during repair by Notch1 signaling via the regulation of vitamin A metabolism. *Dev Cell*. 2007;13(2):242–253.
20. Spits H, Di Santo JP. The expanding family of innate lymphoid cells: regulators and effectors of immunity and tissue remodeling. *Nat Immunol*. 2011; 12(1):21–27.
21. Wynn TA, Ramalingam TR. Mechanisms of fibrosis: therapeutic translation for fibrotic disease. *Nat Med*. 2012;18(7):1028–1040.
22. Bromberg J. Stat proteins and oncogenesis. *J Clin Invest*. 2002;109(9):1139–1142.
23. Levy DE, Lee CK. What does Stat3 do? *J Clin Invest*. 2002;109(9):1143–1148.
24. Levy DE, Darnell JE Jr. Stats: transcriptional control and biological impact. *Nat Rev Mol Cell Biol*. 2002;3(9):651–662.
25. Chan KS, et al. Disruption of Stat3 reveals a critical role in both the initiation and the promotion stages of epithelial carcinogenesis. *J Clin Invest*. 2004; 114(5):720–728.
26. Sano S, et al. Stat3 links activated keratinocytes and immunocytes required for development of psoriasis in a novel transgenic mouse model. *Nat Med*. 2005;11(1):43–49.
27. Kovacic JC, et al. Stat3-dependent acute Rantes production in vascular smooth muscle cells modulates inflammation following arterial injury in mice. *J Clin Invest*. 2010;120(1):303–314.
28. Shouda T, et al. Induction of the cytokine signal regulator SOCS3/CIS3 as a therapeutic strategy for treating inflammatory arthritis. *J Clin Invest*. 2001;108(12):1781–1788.
29. Yasukawa H, et al. IL-6 induces an anti-inflammatory response in the absence of SOCS3 in macrophages. *Nat Immunol*. 2003;4(6):551–556.
30. Wong PK, et al. SOCS-3 negatively regulates innate and adaptive immune mechanisms in acute IL-1–dependent inflammatory arthritis. *J Clin Invest*. 2006;116(6):1571–1581.
31. Song H, Wang R, Wang S, Lin J. A low-molecular-weight compound discovered through virtual database screening inhibits Stat3 function in breast cancer cells. *Proc Natl Acad Sci U S A*. 2005; 102(13):4700–4705.
32. Miyoshi K, et al. Stat3 as a therapeutic target for the

treatment of psoriasis: a clinical feasibility study with STA-21, a Stat3 inhibitor. *J Invest Dermatol*. 2011;131(1):108–117.
33. Laederich MB, et al. The leucine-rich repeat protein LRIG1 is a negative regulator of ErbB family receptor tyrosine kinases. *J Biol Chem*. 2004; 279(45):47050–47056.
34. Shattuck DL, et al. LRIG1 is a novel negative regulator of the Met receptor and opposes Met and Her2 synergy. *Mol Cell Biol*. 2007;27(5):1934–1946.
35. Stutz MA, Shattuck DL, Laederich MB, Carraway KL 3rd, Sweeney C. LRIG1 negatively regulates the oncogenic EGF receptor mutant EGFRvIII. *Oncogene*. 2008;27(43):5741–5752.
36. Cursiefen C, et al. VEGF-A stimulates lymphangiogenesis and hemangiogenesis in inflammatory neovascularization via macrophage recruitment. *J Clin Invest*. 2004;113(7):1040–1050.
37. Sica A, Bronte V. Altered macrophage differentiation and immune dysfunction in tumor development. *J Clin Invest*. 2007;117(5):1155–1166.
38. Biswas SK, Mantovani A. Macrophage plasticity and interaction with lymphocyte subsets: cancer as a paradigm. *Nat Immunol*. 2010;11(10):889–896.
39. Matzinger P, Kamala T. Tissue-based class control: the other side of tolerance. *Nat Rev Immunol*. 2011;11(3):221–230.
40. Weidenbusch M, Anders HJ. Tissue microenvironments define and get reinforced by macrophage phenotypes in homeostasis or during inflammation, repair and fibrosis. *J Innate Immun*. 2012; 4(5–6):463–477.
41. Goldszmid RS, Trinchieri G. The price of immunity. *Nat Immunol*. 2012;13(10):932–938.
42. Mantovani A, Biswas SK, Galdiero MR, Sica A, Locati M. Macrophage plasticity and polarization in tissue repair and remodelling. *J Pathol*. 2013;229(2):176–185.
43. Nakamura T, Endo K, Kinoshita S. Identification of human oral keratinocyte stem/progenitor cells by neurotrophin receptor p75 and the role of neurotrophin/p75 signaling. *Stem Cells*. 2007;25(3):628–638.
44. Nakamura T, et al. Hes1 regulates corneal development and the function of corneal epithelial stem/progenitor cells. *Stem Cells*. 2008;26(5):1265–1274.
45. Nakamura T, et al. The use of trehalose-treated freeze-dried amniotic membrane for ocular surface reconstruction. *Biomaterials*. 2008;29(27):3729–3737.
46. Ueno M, et al. Neural conversion of ES cells by an inductive activity on human amniotic membrane matrix. *Proc Natl Acad Sci U S A*. 2006; 103(25):9554–9559.
47. Nakatsukasa M, et al. Tumor-associated calcium signal transducer 2 is required for the proper subcellular localization of claudin 1 and 7: implications in the pathogenesis of gelatinous drop-like corneal dystrophy. *Am J Pathol*. 2010;177(3):1344–1355.
48. Maruyama K, et al. Inflammation-induced lymphangiogenesis in the cornea arises from CD11b-positive macrophages. *J Clin Invest*. 2005;115(9):2363–2372.
49. Fukuhara S, et al. The sphingosine-1-phosphate transporter Spns2 expressed on endothelial cells regulates lymphocyte trafficking in mice. *J Clin Invest*. 2012;122(4):1416–1426.